

Ballistic and non-ballistic gas flow through ultrathin nanopores

This article has been downloaded from IOPscience. Please scroll down to see the full text article.

2012 Nanotechnology 23 145706

(<http://iopscience.iop.org/0957-4484/23/14/145706>)

View [the table of contents for this issue](#), or go to the [journal homepage](#) for more

Download details:

IP Address: 128.151.150.9

The article was downloaded on 21/03/2012 at 14:21

Please note that [terms and conditions apply](#).

Ballistic and non-ballistic gas flow through ultrathin nanopores

M N Kavalenka¹, C C Striemer^{1,2}, D Z Fang¹, T R Gaborski^{2,3},
J L McGrath³ and P M Fauchet¹

¹ Department of Electrical and Computer Engineering, University of Rochester, Rochester, NY 14627, USA

² SiMPore Inc., West Henrietta, NY 14586, USA

³ Department of Biomedical Engineering, University of Rochester, Rochester, NY 14627, USA

E-mail: fauchet@ece.rochester.edu


Received 15 December 2011, in final form 22 February 2012

Published 21 March 2012

Online at stacks.iop.org/Nano/23/145706

Abstract

We show that ultrathin porous nanocrystalline silicon membranes exhibit gas permeance that is several orders of magnitude higher than other membranes. Using these membranes, gas flow obeying Knudsen diffusion has been studied in pores with lengths and diameters in the tens of nanometers regime. The components of the flow due to ballistic transport and transport after reflection from the pore walls were separated and quantified as a function of pore diameter. These results were obtained in pores made in silicon. We demonstrate that changing the pore interior to carbon leads to flow enhancement resulting from a change in the nature of molecule–pore wall interactions. This result confirms previously published flow enhancement results obtained in carbon nanotubes.

 Online supplementary data available from stacks.iop.org/Nano/23/145706/mmedia

(Some figures may appear in colour only in the online journal)

1. Introduction

Nanoengineered porous membranes have many advantages in lab-on-chip devices, separations/filtrations, nanoelectromechanical and nanofluidic systems applications [1–4], including nanofluidic transistors [5], single-molecule detection [6, 7], DNA sequencing [8] and nanoparticle array fabrication [9]. The primary performance goals of the porous membranes for most applications are high permeation rate and good selectivity, which are achieved by high porosity, narrow pore size distribution and small thickness. Here we describe a novel porous nanocrystalline silicon membrane (pnc-Si) material, in which nanopores are produced by crystallizing a thin amorphous silicon film. Pnc-Si membranes satisfy all of the requirements mentioned above, as they are 15 nm thick with pore diameters ranging from 5 to 50 nm and porosities between 0.1 and 15% [10, 11]. Pnc-Si membranes have been shown to exhibit hydraulic permeability orders of magnitude higher than existing similar membranes [12], demonstrated precise separations of nanoparticles and proteins [12, 13], and

were successfully used for chemical sensing [14, 15] and as cell culture substrates [16].

In addition to their nanotechnological applications, nanoporous membranes often offer an outstanding opportunity to experimentally verify theoretically predicted transport phenomena important for these applications [17–20]. Examples include a detailed study of Knudsen diffusion recently done on electrochemically etched silicon nanochannels [21] and measurement of the conductance of a single nanopore [22]. Knudsen diffusion is a transport regime in which a gas molecule's mean free path exceeds the pore diameter so that molecular collisions with pore walls dominate over intermolecular collisions [23, 24]. In Knudsen diffusion the wall collisions are assumed to be diffusive, meaning that the angle of reflection of the molecule follows Knudsen's cosine law distribution and does not depend on the angle of incidence [23, 25, 26].

Nanofabrication techniques also provide the means to investigate the nature of molecule–pore wall interactions. Maxwell introduced a tangential momentum accommoda-

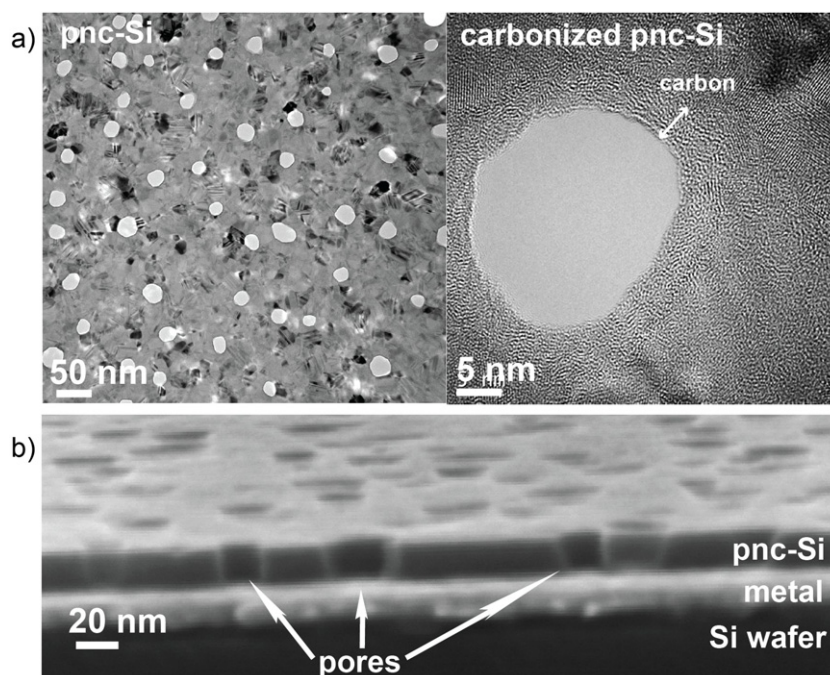


Figure 1. (a) TEM images of pnc-Si and c-pnc-Si membranes. The bright circles are pores and the dark areas are diffracting nanocrystals. The pores in the c-pnc-Si are conformally coated by a carbon layer. (b) Cross-sectional SEM image of the pnc-Si membrane imaged on the surface of the metallized silicon wafer reveals the cylindrical nature of the pores.

tion coefficient (TMAC) that quantitatively describes the molecule–pore wall collisions and defines the fraction of them that undergo diffusive scattering. TMAC is equal to unity for perfectly diffusive collisions (Knudsen regime) and less than unity when specular collisions with pore walls are present [1, 28]. Carbon nanotube (CNT) [29] membranes experience enhanced flow relative to the predictions of the Knudsen model for these membranes [4, 30–32]. This enhancement has been explained by molecular dynamics simulations which suggest that fast transport arises due to the presence of specular molecular collisions with smooth CNT walls [27, 33–36]. TMAC values predicted for CNT are of the order of 10^{-3} [2, 35, 37]. Depositing carbon on the walls of a template porous membrane and annealing it at high temperature has been studied as an alternative to CNTs [2, 37–41]. Cooper *et al* reported a TMAC value of 0.52 ± 0.1 estimated from gas transport studies through carbonized porous alumina membranes [41].

In this paper, we exploit the physical dimensions of the pnc-Si membranes and their dependence on the manufacturing parameters to observe the components of the gas flow, and their dependence on the pore surface. First, we characterize theoretically and experimentally gas transport through molecularly thin pnc-Si membranes. Then we explore the relative contributions of ballistic flow and wall collisions in membranes with different pore sizes, which to the best of our knowledge is the first time these components are observed independently in an experiment. Finally, we deposit a high quality carbon layer on pnc-Si membranes (c-pnc-Si), and compare gas flow through c-pnc-Si and untreated pnc-Si to test whether carbon walls indeed favor specular reflections.

2. Materials and methods

The fabrication of pnc-Si membranes has been described in detail earlier [10, 11]. Resulting pnc-Si membranes are 15 nm thick with pore diameters ranging from 5 to 50 nm and porosities between 0.1 and 15%. Carbonization of pnc-Si membranes is done in a rapid thermal processing (RTP) chamber by introducing acetylene (C_2H_2) for 5 min at 700 °C. Details of this procedure can also be found elsewhere [42].

Transmission electron microscope (TEM) images of pnc-Si and c-pnc-Si are shown in figure 1(a). The nearly circular white areas are open pores in the membrane and the surrounding gray areas correspond to nanocrystalline silicon. The darker areas in the image are nanocrystals with crystal plane alignment satisfying the Bragg condition. Carbonization creates a conformal carbon layer on both sides of the membrane as well as inside the pores. The carbon ring coating pnc-Si pore is shown in figure 1(a). The resulting thickness of c-pnc-Si is ~ 23.5 nm as determined by cross-sectional scanning electron microscope (SEM) images. The cross-sectional SEM of the pnc-Si membrane is illustrated in figure 1(b). Image processing in Matlab [43] is used to directly extract pore sizes and distributions, by first outlining the pore areas and then calculating their diameters d assuming a circular geometry [12] (see supporting information available at stacks.iop.org/Nano/23/145706/mmedia). Using a set of ten $1 \mu m \times 1.7 \mu m$ TEM images from random areas of the same pnc-Si membrane, the estimated standard error is $\sim 2\%$ of the porosity value (e.g. $6.9 \pm 0.16\%$) and less than 1% of the average pore diameter (e.g. 19.6 ± 0.1 nm).

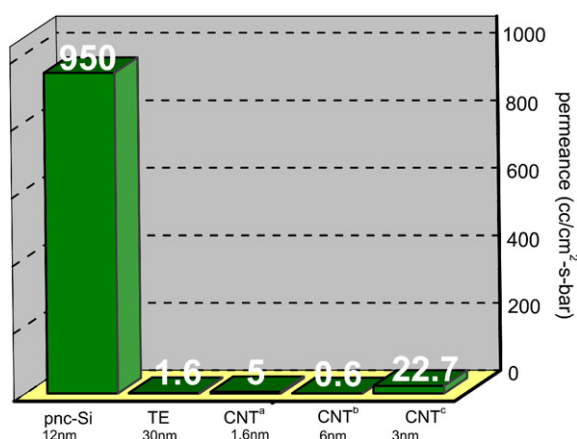


Figure 2. Measured N_2 permeance of pnc-Si membrane, polycarbonate track-etched membrane and reported permeance of three CNT membranes [31, 4, 32]. The pore sizes are indicated in the figure. Experimental values for TE membranes agree with the manufacturer data [44].

Experimental measurements of the gas permeance (N_2 , He, CO_2) were performed using a custom device featuring pnc-Si membranes as in-line filters. The permeance was determined as measured volumetric flow normalized to membrane area and pressure drop. A schematic of the set-up is in the supporting information (available at stacks.iop.org/Nano/23/145706/mmedia). The set-up was also used to test the gas flow rates of commercially available polycarbonate track etch membranes and measured values were in agreement with data provided by the manufacturer [44].

3. Results and discussion

The N_2 permeance of pnc-Si membrane with an average pore diameter of 12 nm is compared to the published permeances of CNT membranes [4, 31, 32] and to our measurements of commercially available polycarbonate track-etched membranes in figure 2. The gas permeance of the ultrathin pnc-Si membrane is several orders of magnitude higher than that of other materials, consistent with permeance measurements in liquids that were recently published [12].

To verify that Knudsen diffusion is the dominant transport mechanism through pnc-Si, we measured N_2 permeance (P) for a large number of pnc-Si membranes with different pore distributions and porosities and compared them to theoretical values predicted for each membrane. The expected molecular flow through a single pore is [3, 23]

$$n = \Delta p A_p / \sqrt{2\pi MRT} (1 + L/2r)^{-1} \quad (1)$$

where Δp is the differential pressure, A_p is the pore area, M is the gas molar mass, L is the length and r is the pore radius. The flow in equation (1) is defined as the rate at which molecules enter an opening of an area A_p with an adjustment for the restrictions caused by the pore walls. This adjustment is introduced by the Clausing factor W (approximated transmission probability), which for a short tube-shaped pore is given by $W = (1 + L/2r)^{-1}$ [18, 19, 24, 45].

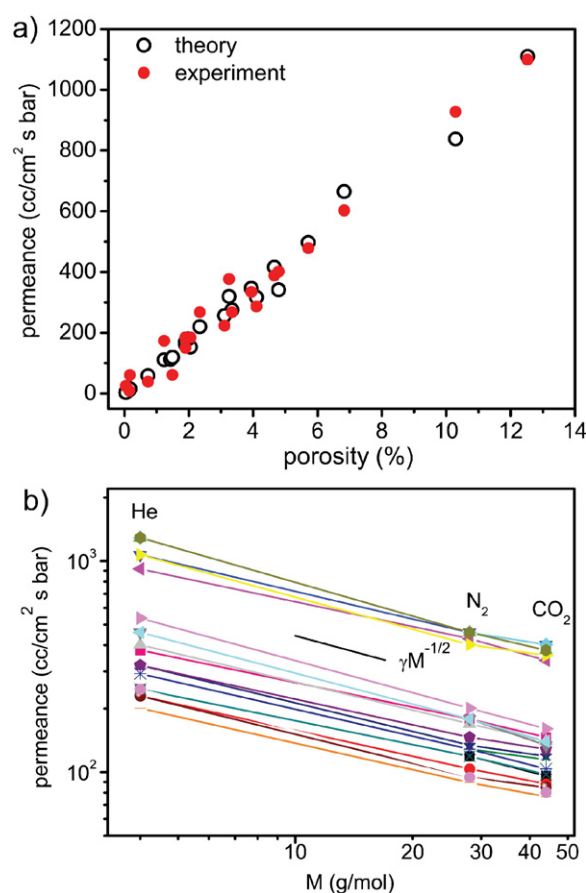


Figure 3. (a) Experimental and theoretical N_2 permeance of pnc-Si membranes with different porosities and pore size distributions. (b) Measured N_2 , He and CO_2 permeance as a function of molar mass M . Lines represent measurements on 22 different pnc-Si membranes, while the average slope of fitted lines is -0.45 ± 0.05 . The line of slope $-1/2$ is a guide for the eyes.

To determine the theoretical permeance of a particular membrane, the TEM image of that membrane was first processed to extract pore size histograms. The molecular flow through each pore in the image was calculated using equation (1). The permeance was then calculated by summing the flow rates through the individual pores and normalizing the sum by the pressure drop and the active area of the membrane. Experimental and theoretical permeance values for pnc-Si membranes with porosities ranging from 0.1% to 15% and different pore distributions are illustrated in figure 3(a). The cutoff pore diameters for the tested membranes ranged from 25 to 55 nm. Figure 3(a) demonstrates the excellent agreement between Knudsen theory and experiments for individual pnc-Si membranes.

To further investigate the transport mechanism, we also tested the Knudsen scaling prediction that permeance increases with the inverse square root of the molar mass of the gas [3, 30]. The measured pnc-Si permeance values for N_2 , He and CO_2 shown in figure 3(b) are in agreement with the Knudsen scaling prediction. Additionally, the experimental selectivity α expressed as the ratio of gas permeances is in agreement with Knudsen selectivity coefficients $\alpha = \sqrt{M_{\text{gas2}}/M_{\text{gas1}}}$ for CO_2/N_2 , N_2/He and CO_2/He pairs [46,

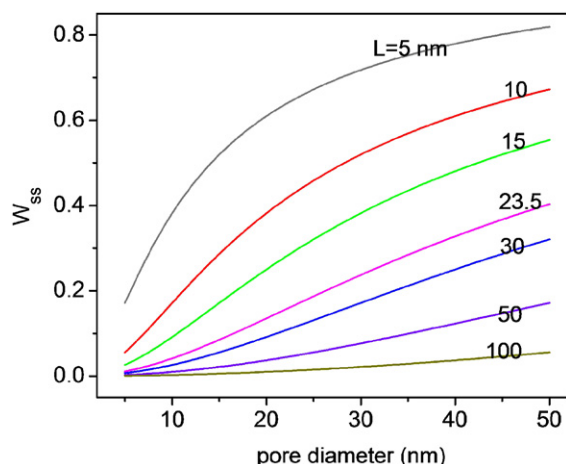


Figure 4. Ballistic flow component W_{ss} for pores of different diameters and lengths (equation (3)).

47]. Finally, the measured permeance is independent of feed pressure, demonstrating that the contribution of viscous flow is negligible [46, 48]. Details of these two studies are in the supporting information (available at stacks.iop.org/Nano/23/145706/mmedia). The agreement between transport experiments and theory indicates that Knudsen diffusion accurately describes transport through pnc-Si. Thus the molecular collisions with pnc-Si pore walls are diffusive [31, 49, 50].

In 1932 Clausing formalized the concept of a transmission probability W as the fraction of incoming gas molecules that pass through a pore without being reflected back [18]. The integral equation that calculates W considers all possible molecular trajectories and decouples the flow into two probabilities: the probability that a molecule passes the pore without encountering the pore wall, W_{ss} (ballistic component) and the probability of transport through the pore after some collision with the wall, W_{wall} (wall collision component) [18, 51]. In the Knudsen regime, the transmission probability of a cylindrical tube of length L is given by [18, 51]

$$W = W_{ss}(L) + \int_0^L W_{sr}(x)w(x) dx, \quad (2)$$

where the function W_{ss} is the probability of the molecule passing the tube without colliding with the wall (i.e. the ballistic component). The second term in equation (2) (the wall component W_{wall}) represents the probability that a molecule will pass through the pore after colliding with the wall. The function $w(x)$ is defined by the Clausing integral equation $w(x) = W_{rs}(L-x) + \int_0^L W_{rr}(x'-x)w(x') dx'$ and equals the flux density striking the wall at position x . The functions $W_{sr}(x)$, $W_{rs}(L-x)$, $W_{rr}(x'-x)$ represent the probabilities that a molecule reflected from the wall at different positions will exit the pore. The ballistic component $W_{ss}(L)$ is given by a geometric factor [18, 51, 52]

$$W_{ss} = (L^2 - L\sqrt{L^2 + 4r^2} + 2r^2)/2r^2. \quad (3)$$

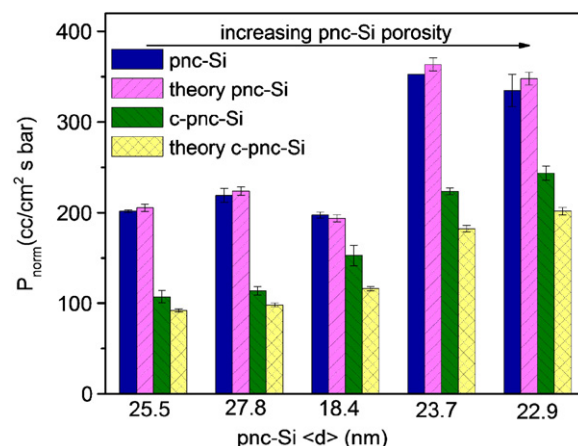


Figure 5. Experimental P of pnc-Si membranes from five different wafers before and after carbonization compared to theoretical Knudsen predictions. Initial wafer porosities are: 2.5%, 2.87%, 3.25%, 4.97% and 5.09%. Corresponding average pore diameters and porosities after carbonization: 20.5 nm, 1.34%; 21.3 nm, 1.3%; 17.1 nm, 1.91%; 18.5 nm, 2.86%; and 20.7 nm, 2.87%. Pnc-Si and c-pnc-Si thicknesses are 15 nm and 23.5 nm.

The dependence of the ballistic component W_{ss} on length L and diameter d is plotted in figure 4. The fraction of flow due to molecules with ballistic trajectories increases as pores become wider and shorter. For 15 nm thick membranes, 40 nm pores result in $W_{ss} = 0.48$ whereas 10 nm pores result in $W_{ss} = 0.09$ [18]. The ballistic component for membranes thicker than 50 nm becomes negligible unless the pores are significantly larger than the membrane thickness. When either the pore size or thickness approaches the mean free path λ at standard conditions (~ 70 nm), molecular collisions become more likely and the assumption of molecular flow upon which the Clausing formulations are based is no longer valid.

In order to experimentally determine the W_{ss} and W_{wall} components, we examined the measured flow through pnc-Si and carbonized pnc-Si membranes. Figure 5 compares the experimental and theoretical permeance for five membranes before and after carbonization. The measured permeance values for pnc-Si agree with theory. While a decrease in porosity and increase in thickness after pnc-Si carbonization result in lower permeance, the experimental results for c-pnc-Si are significantly larger than predicted by Knudsen diffusion, assuming diffusive reflections.

To extract the impact of pore diameter in membranes of different porosities, we divided experimental permeance values by porosity to create a normalized permeance P_{norm} and this data is plotted in figure 6. To allow the direct comparison of coated c-pnc-Si (solid squares) and non-coated pnc-Si (solid circles) membranes, P_{norm} values for 23.5 nm thick pnc-Si were extrapolated from results obtained for 15 nm pnc-Si using the Clausing factor $W = (1 + L/2r)^{-1}$ [18, 19, 24, 45], which lowered P_{norm} by 12 cc/cm² s bar on average. For both pnc-Si and c-pnc-Si, the increase in P_{norm} as a function of average pore diameter seen in figure 6 is due to the increasing contribution of ballistic flow at larger pore sizes as shown in figure 4. To the best of our knowledge this is

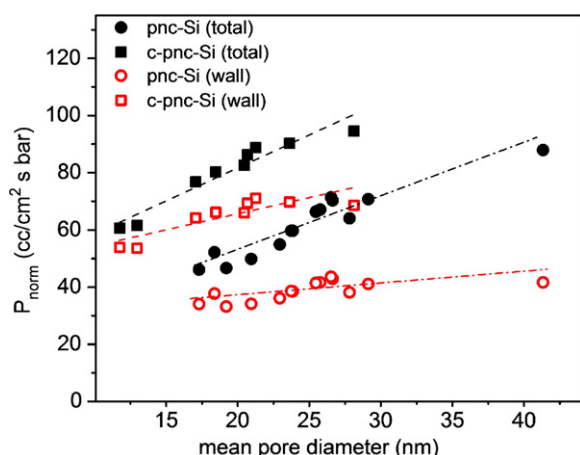


Figure 6. Experimental P_{norm} of 23.5 nm thick pnc-Si and c-pnc-Si membranes plotted against mean pore diameter. The wall component of P_{norm} is found by subtracting the calculated W_{ss} component from the total measured P_{norm} . The error in the wall components of P_{norm} due to the pore size distribution is less than 0.5%. The dashed lines are least-squares fits.

the first time the ballistic component of the gas flow has been explicitly observed.

Flow enhancement at all pore diameters is clearly observed in the carbonized membranes in figure 6. We calculated the permeances due to W_{wall} by subtracting the ballistic component for the corresponding mean pore diameter using equation (3) from the total measured flow [23, 46] (see supporting information available at stacks.iop.org/Nano/23/145706/mmedia). We find that the wall component accounts for all the enhancement in the c-pnc-Si flow (open squares—figure 6). Our analysis of flow components provides strong evidence that carbonization enhances gas flow by changing the nature of the molecule–pore wall interactions from diffusive to more specular, consistent with the high quality and graphene-like structure observed after high temperature carbonization [38–41, 2, 42] and with reported flow enhancements in CNTs.

4. Conclusion

In conclusion, we demonstrated that gas permeance in ultrathin pnc-Si membranes is orders of magnitude higher than in membranes which have similar pore sizes. We directly observed two aspects of molecular flow through pores whose diameters and lengths are less than the mean free path of gas molecules. First, we found a significant contribution of the ballistic component to the total permeance of pnc-Si, due to the unique geometry of this nanoporous ultrathin material. Second, we demonstrated an enhancement in permeance caused by changing the pore wall surface from one that scatters diffusely to one that scatters in a more specular fashion. This enhancement occurred after high temperature carbonization was used to deposit carbon inside the pores of pnc-Si and is consistent with the molecular flow enhancement reported in CNTs.

Acknowledgments

We acknowledge Professor M Anthamatten for useful discussions and the National Science Foundation for support of this work under grants DMR0722653 and ECCS0707795.

References

- [1] Karniadakis G, Beskok A and Aluru N 2005 *Microflows and Nanoflows: Fundamentals and Simulation* (New York: Springer)
- [2] Whitby M and Quirke N 2007 *Nature Nanotechnol.* **2** 87
- [3] Tong H, Jansen H, Gadgil V, Bostan C, Berenschot E, van Rijn C and Elwenspoek M 2004 *Nano Lett.* **4** 283
- [4] Hinds B, Chopra N, Rantell T, Andrews R, Gavalas V and Bachas L 2004 *Science* **303** 62
- [5] Nam S-W, Rooks M J, Kim K-B and Rossmagel S M 2009 *Nano Lett.* **9** 2044
- [6] Yusko E C, Johnson J M, Majd S, Prangkio P, Rollings R C, Li J, Yang J and Mayer M 2011 *Nat. Nanotechnol.* **6** 253
- [7] Wei R, Pedone D, Zurner A, Doblinger M and Rant U 2010 *Small* **6** 1406
- [8] Singer A, Wanunu M, Morrison W, Kuhn H, Frank-Kamenetskii M D and Meller A 2010 *Nano Lett.* **10** 738
- [9] Sander M S and Tan L-S 2003 *Adv. Funct. Mater.* **13** 393
- [10] Striemer C C, Gaborski T R, McGrath J L and Fauchet P M 2007 *Nature* **445** 749
- [11] Fang D Z, Striemer C C, Gaborski T R, McGrath J L and Fauchet P M 2010 *J. Phys.: Condens. Matter* **22** 454134
- [12] Gaborski T R, Snyder J L, Striemer C C, Fang D Z, Hoffman M, Fauchet P M and McGrath J L 2010 *ACS Nano* **4** 6973
- [13] Snyder J L, Clark A Jr, Fang D Z, Gaborski T R, Striemer C C, Fauchet P M and McGrath J L 2010 *J. Membr. Sci.* **369** 119
- [14] Kavalenka M N, Striemer C C, Fang D Z, Gaborski T R, McGrath J L and Fauchet P M 2009 *Active polymers, Mater. Res. Soc. Symp. Proc. (San Francisco, CA 2009)* p 1190
- [15] Kavalenka M N, Striemer C C, DesOrmeaux J-P S, McGrath J L and Fauchet P M 2012 *Sensors Actuators B* **162** 22
- [16] Agrawal A A, Nehilla B J, Reisig K V, Gaborski T R, Fang D Z, Striemer C C, Fauchet P M and McGrath J L 2010 *Biomaterials* **31** 5408
- [17] Knudsen M 1909 *Ann. Phys.* **28** 75
- [18] Clausing P 1932 *Ann. Phys.* **12** 961
- [19] Dushman S and Lafferty J M 1962 *Scientific Foundations of Vacuum Technique* (New York: Wiley)
- [20] Graham T 1846 *Phil. Trans. R. Soc.* **136** 573
- [21] Gruener S and Huber P 2008 *Phys. Rev. Lett.* **100** 064502
- [22] Savard M, Tremblay-Darveau C and Gervais G 2009 *Phys. Rev. Lett.* **103** 104502
- [23] Elwenspoek M and Jansen H 1998 *Silicon Micromachining* (Cambridge: Cambridge University Press)
- [24] Steckelmacher W 1986 *Rep. Prog. Phys.* **49** 1083
- [25] Valleau J P, Diestler D J, Cushman J H, Schoen M, Hertzner A W and Riley M E 1991 *J. Chem. Phys.* **95** 6194
- [26] Albo S E, Broadbelt L J and Snurr R Q 2006 *AIChE J.* **11** 3679
- [27] Bhatia S K, Haibin C and Sholl D S 2005 *Mol. Simul.* **9** 643
- [28] Sokhan V P and Quirke N 2008 *Phys. Rev. E* **78** 01530
- [29] Iijima S 1991 *Nature* **354** 56
- [30] Kim S, Jinschek J R, Chen H, Sholl D S and Marand E 2008 *Nano Lett.* **7** 2806
- [31] Holt J, Park H, Wang Y, Stadermann M, Artyukhin A, Grigoropoulos C, Noy A and Bakajin O 2006 *Science* **312** 1034

- [32] Yu M, Funke H H, Falconer J L and Noble R D 2009 *Nano Lett.* **9** 225
- [33] Skoulidas A I, Ackerman D M, Johnson J K and Sholl D S 2002 *Phys. Rev. Lett.* **89** 185901
- [34] Chen H and Sholl D S 2006 *J. Membr. Sci.* **269** 152
- [35] Sokhan V P, Nicholson D and Quirke N 2002 *J. Chem. Phys.* **117** 8531
- [36] Arya G, Chang H-C and Maginn E J 2003 *Mol. Simulat.* **29** 697
- [37] Noy A, Park H G, Fornasiero F, Holt J K, Grigoropoulos C P and Bakajin O 2007 *Nano Today* **2** 22
- [38] Mattia D, Rossi M, Kim B, Korneva G, Bau H and Gogotsi Y 2006 *J. Phys. Chem. B* **110** 9850
- [39] Miller S A, Young V Y and Martin C R 2001 *J. Am. Chem. Soc.* **123** 12335
- [40] Che G, Lakshmi B B, Fisher E R and Martin C R 1998 *Nature* **393** 346
- [41] Cooper S M, Cruden B A and Meyyappan M 2004 *Nano Lett.* **4** 377
- [42] Fang D Z, Striemer C C, Gaborski T R, McGrath J L and Fauchet P M 2010 *Nano Lett.* **10** 3904
- [43] MATLAB code available for download at www.nanomembranes.org/software.html
- [44] www.sterlitech.com
- [45] Unnikrishnan S, Jansen H V, Falke F H, Tas N R, Van Wolferen H A G M, De Boer M J, Sanders R G P and Elwenspoek M C 2009 *Nanotechnology* **20** 305304
- [46] Verweij H, Schillo M C and Li J 2007 *Small* **3** 1996
- [47] Martin C, Nishizawa M, Jirage K and Kang M 2001 *J. Phys. Chem. B* **105** 1925
- [48] Pages X, Rouessac V, Cot D, Nabias G and Durand J 2001 *Sep. Purif. Tech.* **25** 399
- [49] Ruthven D M, DeSisto W J and Higgins S 2009 *Chem. Eng. Sci.* **64** 3201
- [50] Leger C, Lira H De L and Paterson R 1996 *J. Membr. Sci.* **120** 135
- [51] Helmer J C 1967 *J. Vac. Sci. Technol.* **4** 179
- [52] Levi G, Simon M D and Helmer J C 1995 *Vacuum* **46** 357